# Fatigue damage behavior of a surface-mount electronic package under different cyclic applied loads*

Ren Huai-Hui(任淮辉)[a)b)†] and Wang Xi-Shu(王习术)[b)]

[a)] *Longyuan (Beijing) Wind Power Engineer Technology Co. Ltd, Beijing* 100034, *China*

[b)] *Department of Engineering Mechanics, Tsinghua University, Beijing* 100084, *China*

(Received 4 June 2013; revised manuscript received 25 August 2013; published online 10 February 2014)

This paper studies and compares the effects of pull–pull and 3-point bending cyclic loadings on the mechanical fatigue damage behaviors of a solder joint in a surface-mount electronic package. The comparisons are based on experimental investigations using scanning electron microscopy (SEM) *in-situ* technology and nonlinear finite element modeling, respectively. The compared results indicate that there are different threshold levels of plastic strain for the initial damage of solder joints under two cyclic applied loads; meanwhile, fatigue crack initiation occurs at different locations, and the accumulation of equivalent plastic strain determines the trend and direction of fatigue crack propagation. In addition, simulation results of the fatigue damage process of solder joints considering a constitutive model of damage initiation criteria for ductile materials and damage evolution based on accumulating inelastic hysteresis energy are identical to the experimental results. The actual fatigue life of the solder joint is almost the same and demonstrates that the FE modeling used in this study can provide an accurate prediction of solder joint fatigue failure.

**Keywords:** solder joint, fatigue life, hysteresis energy, SEM *in-situ* technology

**PACS:** 46.50.+a, 74.25.Jb, 62.20.M– **DOI:** 10.1088/1674-1056/23/4/044601

## 1. Introduction

With the continuous development of the electronics package industry, customers are making increasing demands on electronic components and packaging technology, such as miniaturization, fatigue reliability, and impact resistance. In the past several decades, researchers have mainly paid close attention to the investigation of electromigration failures and thermal cyclic fatigue reliability, and the failure or reliability analyses for the electric circuits or packages have been widely carried out by using *in-situ* measurements of the electric resistance changes for the total circuit board.[1–4] However, the mechanical cyclic fatigue, which is often caused by the mechanical oscillations in the large-scale integrated circuit boards or micro-electro-mechanical systems of the served equipment[5] or supervenes the thermal cyclic loading synchronously,[6,7] is ignored. So comprehensively understanding the multi-scale or micro-scale fatigue failure mechanism of solder joints in a surface-mount electronic package under different cyclic applied loads will be a challenge.

The aim of this paper is to study the effects of axial tensile and 3-point bending loading tests ($R = \sigma_{\min}/\sigma_{\max} = 0.1$, $R$ is the stress ratio, $\sigma_{\min}$ is the minimum value, and $\sigma_{\max}$ is the maximum value in the cyclic stress) on the high cyclic fatigue (HCF) crack initiation and propagation behavior of the solder joint in the packaging system of chip-solder-land-substrate. Scanning electron microscopy (SEM) *in-situ* observation technology is used to detect the fatigue crack initiation and propagation behavior of the solder joint, and the fatigue crack morphology of a solder joint subjected to the different loading cycles is completely recorded, so HCF lifes of solder joint under the different applied loads are deduced. In addition, finite element (FE) modeling under the different applied loads is carried out to obtain the stress–strain response relations for the solder joint with different components in the static analysis and investigate the fatigue damage initiation and evolution process of the solder joint in the direct cyclic and fatigue analysis. The constitutive model of damage initiation criteria for ductile materials and damage evolution based on accumulating inelastic hysteresis energy is defined to characterize the material property of the solder joint.

## 2. Experimental cyclic tests

Both of the fatigue tests under two cyclic applied loads with the same stress ratio of $R = 0.1$ ($R = \sigma_{\min}/\sigma_{\max}$) were conducted on a simple surface-mount electronic assembly with a chip, solder, Cu land, and substrate as shown in Fig. 1. The pull–pull axial cyclic loading parallel to the axial direction of substrate is defined in the tensile tests (see Fig. 1(a)), and the push–push bending cyclic loading perpendicular to the axial direction of substrate in the bending tests is shown in Fig. 1(b). For the two kinds of cyclic loading tests, the configurations of the samples are very different, and the detailed dimensions are marked in Fig. 1. All samples without any processing were employed directly in order to find the exact failure cause under different applied loads.

*Project supported by the National Basic Research Program of China (Grant No. 2010CB631006) and the National Natural Science Foundation of China (Grant Nos. 11072124 and 11272173).

†Corresponding author. E-mail: renhuaihui@foxmail.com

© 2014 Chinese Physical Society and IOP Publishing Ltd 

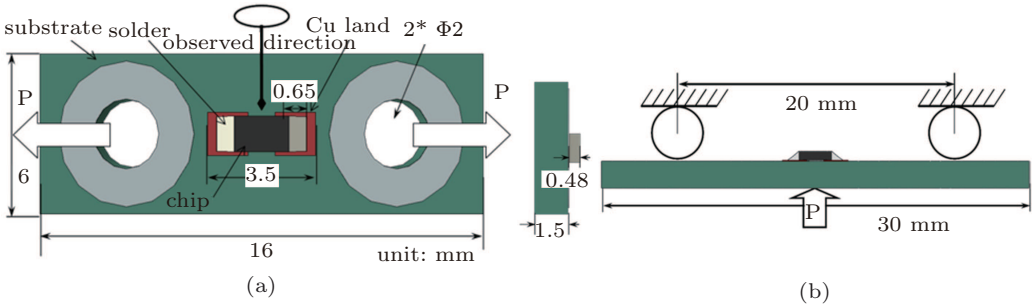



**Fig. 1.** (color online) SEM *in-situ* observation images of specimens: (a) pull–pull loading and (b) 3-point bending cyclic loading.

The fatigue tests were carried out by using a servo-hydraulic testing stage, which was placed in the vacuum chamber in the SEM system.[8–11] Pull–pull and 3-point bending cyclic loadings were applied directly to the substrate as shown in Fig. 1, respectively. The mechanical testing stage can provide pulsating (sine wave) loading at 10 Hz of $\pm 1$ kN maximum capacity and a displacement region of $\pm 25$ mm. Stresses were controlled in these fatigue tests, the maximum normal stress of about 70 MPa with a stress ratio of $R = 0.1$ was applied to the substrate. Because most initial fractures of the solder joint occurred at the heels or toes of the solder joint, as indicated in Refs. [12]–[14], the SEM *in-situ* observation was focused on these positions. The SEM images were taken at random cycles. The free surface fatigue crack propagation paths were detected directly with the calibrated scale of an SEM *in-situ* system. The SEM images of small fatigue cracks were recorded at maximum applied loading in sine wave and at a frequency of 0.01 Hz. Subsequently, the loading frequency was increased up to 8 Hz to accelerate the fatigue damage process. In this work, the HCF ranges for solder joints are defined as being from $2 \times 10^4$ to $2 \times 10^6$ cycles according to the requirements in the solder joint's practical application.

## 3. Numerical simulation of surface-mount package

### 3.1. Finite element modeling of surface-mount package

In general, the fatigue process simulation includes three analysis procedures: static analysis under the mean stress of $\sigma_m = (\sigma_{max} + \sigma_{min})/2.0$ for the substrate (but the maximum stress $\sigma_{max} = 70.0$ MPa) was carried out at first. Based on the static analysis, the direct cyclic analysis was performed to obtain the stabilized response of solder joint under two different cyclic applied loads with a pulsating (sine wave) amplitude of $\sigma_a = 22.5$ MPa for the substrate ($\sigma_a = (\sigma_{max} - \sigma_{min})/2.0$ is an amplitude of stress), subsequently fatigue analysis using the direct cyclic approach was carried out to simulate the damage initiation and evolution of the solder joint, and the damage accumulation and damage extrapolation technique in the ductile material was used to accelerate the damage failure of the solder joint.[15,16]

The FE models of three-dimensional (3D) chip-solder-land-substrate for pull–pull and 3-point bending applied loads are shown in Fig. 2. The local grids were refined enough for the possible damage region of the solder joint including the Cu land and chip as shown in Fig. 2(a), and there are the same grids for two FE models with the different applied loads in this region. About 83052 second-order 3D hexahedral elements were employed to mesh the geometric model of the solder joint. For the axial tensile loading, the reference point was created to couple the six nodes with degrees of freedom of bolt holes in the experiment, and about 320 N of reaction forces in static analysis was exerted on the reference point along the axial direction of substrate, as shown in Fig. 2(a). Then the pull–pull sine pulsating cyclic loading based on this mean loading and $R = 0.1$ were defined in direct cyclic and fatigue analysis. For the 3-point bending loading, in order to be suitable for the loading ranges of the experimental facilities, the thickness of substrate was doubled. A nonlinear FE model, which is considered as the contact analysis between the substrate and the rigid punch die, was created as shown in Fig. 2(b). Two bottom punch dies were fixed, and an about 118-N reaction force in static analysis was exerted on the upper punch die. The push–push bending cyclic loading was defined just like the axial tensile loading.

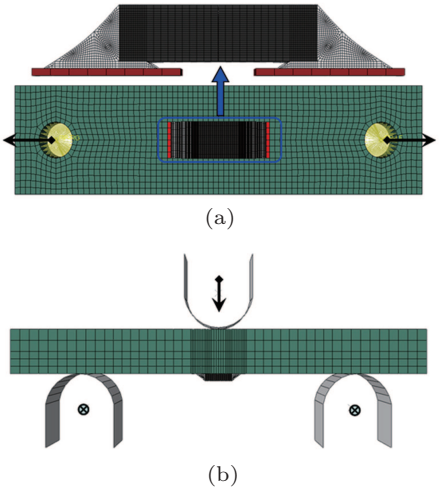



**Fig. 2.** (color online) FE modeling and meshes of surface-mount electronics packages: (a) pull–pull loading and (b) 3-point bending cyclic loading.

### 3.2. Material constitutive model of the solder joint

In the FE modeling, the chip is made (2A-0805 type) of RN73S, the solder is 63Sn-37Pb, and the substrate of the printed circuit board (PCB) is the FR-4 epoxy/glass composite panel. To connect the solder and the PCB substrate effectively, a smaller Cu plate (land-size) was embedded into the substrate surface. For the static analysis, elastic constitutive models of all components were used.[17] However, for the direct cyclic and fatigue analysis, kinematic hardening models were used to simulate the inelastic behavior of materials that were subjected to cyclic loading. So the plastic properties with kinematic hardening need to be defined.

In addition, the constitutive equations of SnPb alloy under cyclic loading at room temperature could be characterized as follows:[4,7]

$$\Delta\sigma = 1.71\times10^{5}\Delta\varepsilon^{1.47} \text{ or } \Delta\sigma = 1.85\times10^{5}\Delta\varepsilon_{\mathrm{p}}^{1.44}, \quad (1)$$

$$\dot{\varepsilon} = 5.15\times10^{-10}\sigma_{\mathrm{b}}^{4.76}, \quad (2)$$

where $\Delta\sigma$ and $\Delta\varepsilon$ are the stress and strain range of bulk SnPb solder, respectively, $\Delta\varepsilon_{\mathrm{p}}$ is the plastic strain range, $\dot{\varepsilon}$ is the strain rate, and $\sigma_{\mathrm{b}}$ is the yield stress of SnPb alloy. As in our previous results reported in Refs. [4], [12]–[14], for the fatigue failure of solder joint, both of the damage initiation criteria for ductile materials and the damage evolution based on accumulating inelastic hysteresis energy for the solder joint were considered in this simulation. Because the computational cost to simulate the slow progressive damage in a material over many load cycles is prohibitively expensive except for the case of the simplest models, numerical fatigue life studies usually involve modeling the response of the structure subjected to a small fraction of the actual loading history. The direct cyclic analysis capability provides a computationally effective modeling technique to obtain the stabilized response of a structure subjected to periodic loading and is ideally suited to the fatigue calculations on a large structure. The capability uses a combination of Fourier series and time integration of the nonlinear material behavior to obtain the stabilized response of the structure directly, as shown in Fig. 3(a); then the material point of the structure turns into the damage status, and the cycle number in which damage is initiated is given as follows:

$$N = c_1\Delta w^{c_2}, \quad (3)$$

where $c_1$ and $c_2$ are material constants, and determined to be 78 and $-1.44$, respectively, $\Delta w$ is the accumulating inelastic hysteresis energy per cycle.

If the damage initiation criterion is satisfied at any material point at the end of a stabilized cycle, $N$, the fatigue analysis will extrapolate the damage variable $D_N$ from the current cycle forward to the next increment over a number of cycles, $\Delta N$. The new damage state, $D_{N+\Delta N}$, is given by

$$D_{N+\Delta N} = D_N + \frac{\Delta N}{L}c_3\Delta w^{c_4}, \quad (4)$$

where $L$ is the characteristic length associated with an integration point, and $c_3$ and $c_4$ are the material constants, and determined to be $4.8768\times10^{-8}$ and 1.05, respectively.

This response is then extrapolated over many load cycles using empirical formulae such as the Coffin–Manson relationship to predict the likelihood of crack/damage initiation and propagation, which can assist the model to accelerate the FE analysis of fatigue damage.[17,18] The damage evolution law describes the rate of degradation of the material stiffness per cycle once the corresponding initiation criterion has been reached as shown in Fig. 3(b). The degradation of the stiffness can be modeled using a scalar damage variable, $D$. At any given cycle during the analysis the stress tensor in the material is given by the scalar damage equation

$$\sigma = (1-D)\bar{\sigma}, \quad (5)$$

where $\bar{\sigma}$ is the effective (or undamaged) stress tensor that would exist in the material in the absence of damage computed in the current increment. The material has lost its load carrying capacity when $D = 1$.

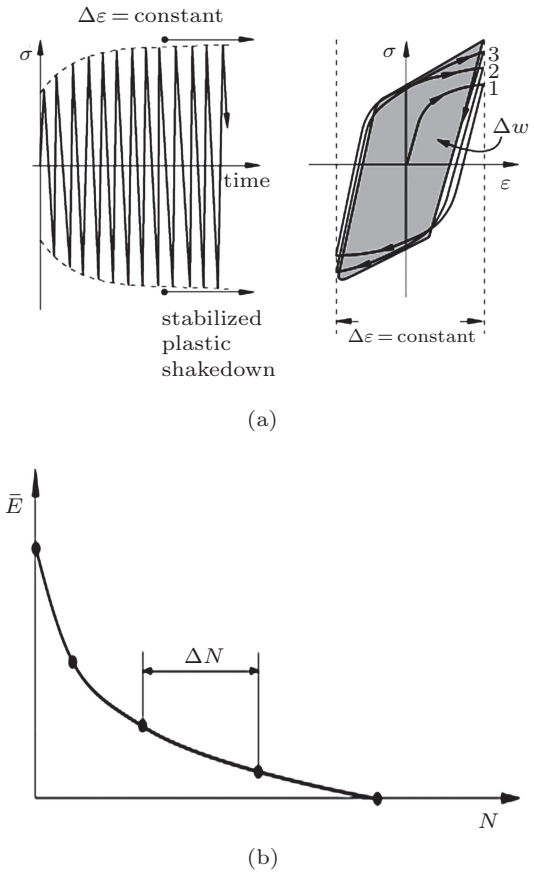



**Fig. 3.** Constitutive model of the solder joint: (a) plastic shakedown in a direct cyclic analysis and (b) elastic stiffness degradation as a function of cycle number.

## 4. Results and discussion

### 4.1. Stress and strain fields of the typical solder joints

As previously mentioned, the static analysis of FE models for the two applied loads was carried out at first in order to understand the concentrative location of the stress and strain. We assume that all interfaces of the different components of surface-mount electronic package each have a compatible strain field when the normal stress of substrate is given as a constant. The von Mises stress distributions in the chip, solder joint, and Cu land under pull–pull loading and 3-point bending cyclic loading of the substrate can be obtained as shown in Figs. 4(a) and 4(b), respectively. The results indicated that for two different applied loads, the positions of maximum Mises stress all occurred in the chip and the interfaces between the chip and the solder joints.[19] The difference is that the axial tensile loading resulted in the stress concentration at the heel and the toe located in the interface of the solder joint. However, for the 3-point bending cyclic loading, the extensive regions of the stress concentration occurred at the heel of the solder joint. In order to represent the stress variation on the surface of the solder joint, three paths were selected to record the Mises stress, and the selected nodes under the chip were the same. The relation curves (see Figs. 4(c) and 4(d)) of the paths and the stress for the different applied loads indicate that the maximum stress (68.02 MPa) for the pull–pull loading is greater than the one for the 3-point bending cyclic loading (63.96 MPa), and there is an inflection point near the toe below the chip, the average Mises stresses on these paths for bending loading are obviously greater. The greatest difference is the rates of decline along the three paths, which will determine the different failure modes and fatigue lifetimes of the solder joint under the different applied loads. The single crack propagation for the axial loading, the cumulative damage to the local regions of the solder joints, and the crack propagation for the bending loading can be predicted. So the failure modes for the bending loading are more complex and comprehensive. This is because the solder alloy has a ductile fracture characteristic. Therefore, the effects of different applied loads on the change of stress concentrative region cannot be ignored.

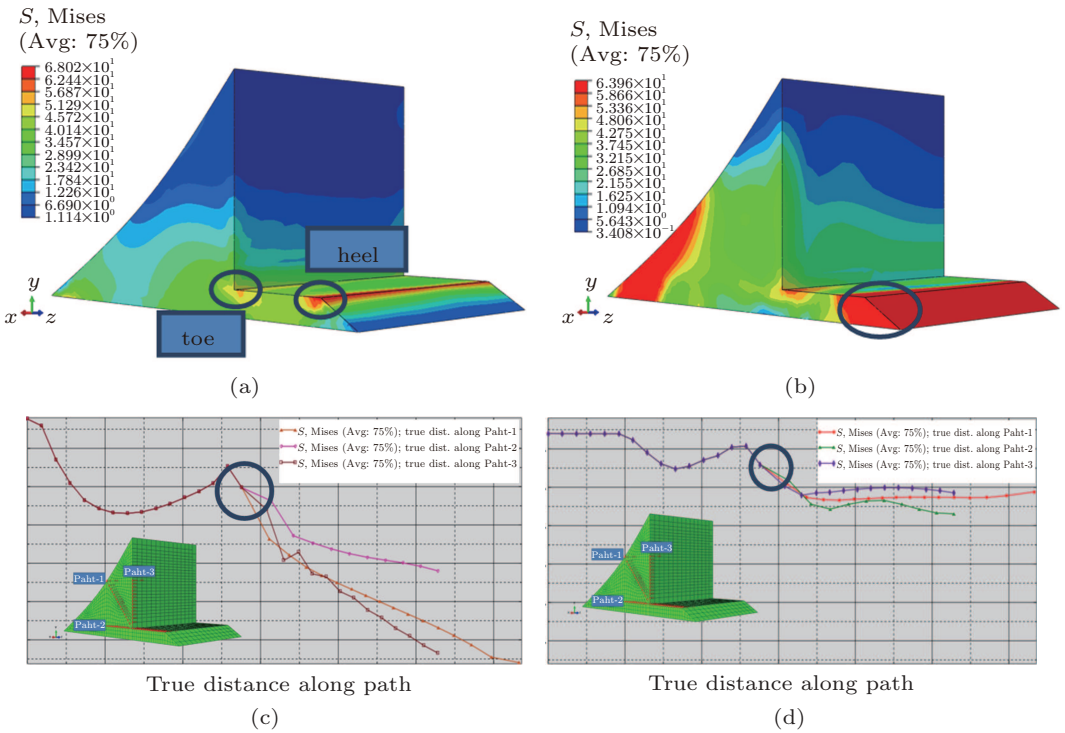



**Fig. 4.** (color online) Results of stress at the solder joint and the relation curves of stress and three paths in the static analysis: (a) Mises stress distribution for tensile loading, (b) Mises stress distribution for bending loading, (c) the relation curves under pull–pull loading, and (d) the relation curves under 3-point bending cyclic loading.

### 4.2. Comparison results between the experiment and simulation

In terms of the results of static analysis for two applied loads, the cyclic loading amplitudes were calculated by the reaction force of constraint node. Thus, the applied load forces were used in the experiment, and the quantitative characterization of fatigue crack initiation and propagation behavior of the solder joint should be validated by the SEM *in-suit* observation.[20,21] In addition, according to the results of static analysis and observation in the experiment, we find that the fatigue failure propagation is driven by the plastic strain or shear stress at the tip of the solder joint.[22] The direct cyclic analysis can easily make the plastic strain reach a stabilized state under the periodic cyclic loading by controlling the number

of Fourier terms instead of a large number of redundant incremental iterations (see Fig. 2(a)), then fatigue analysis using the damage extrapolation technique was carried out based on the cyclic direct analysis. Some skills are usually used to facilitate the computing convergence and collect the analysis results after the different cycles. For example, the reasonable minimum ($\Delta N_{\min}$) and maximum ($\Delta N_{\max}$) number of cycles over which the damage is extrapolated forward in any given increment was specified, or the restart analysis is often employed between two different cycles. A non-dimensional parameter, called scalar stiffness degradation, which is represented by SDEG in this analysis, was used to characterize the damage level of SnPb solder after the different cycles when the applied loading was a constant.

For the pull–pull axial cyclic loading, the sample was inverted to be suitable for installation, the bottom solder joint was observed primarily, and the corresponding regions with fatigue cracks were magnified as shown in Fig. 5(a). For the fatigue crack early-stage growth behavior, a very small fatigue crack initiation mainly occurred at the interface between the chip and the solder joint before 6994 cycles, which can be verified from the FE fatigue analysis as shown in Fig. 5(b). The simulation results indicate that local damage appeared at the toe and the heel, and with the continuous accumulation of small plastic strain at the interface, fatigue crack growth occurred at the toe of the solder joint and began a new journey from the toe; after 10106 cycles the length of crack reached about 35.6 μm as shown in Fig. 5(c). Accordingly, the damage evolution process of the scalar stiffness degradation along the interface of solder and chip is shown in Fig. 5(d) after $1 \times 10^5$ cyclic tensile loadings. The crack growth direction along the 45° of the solder joint indicated that the results of the experiment and the FE simulations matched very well.

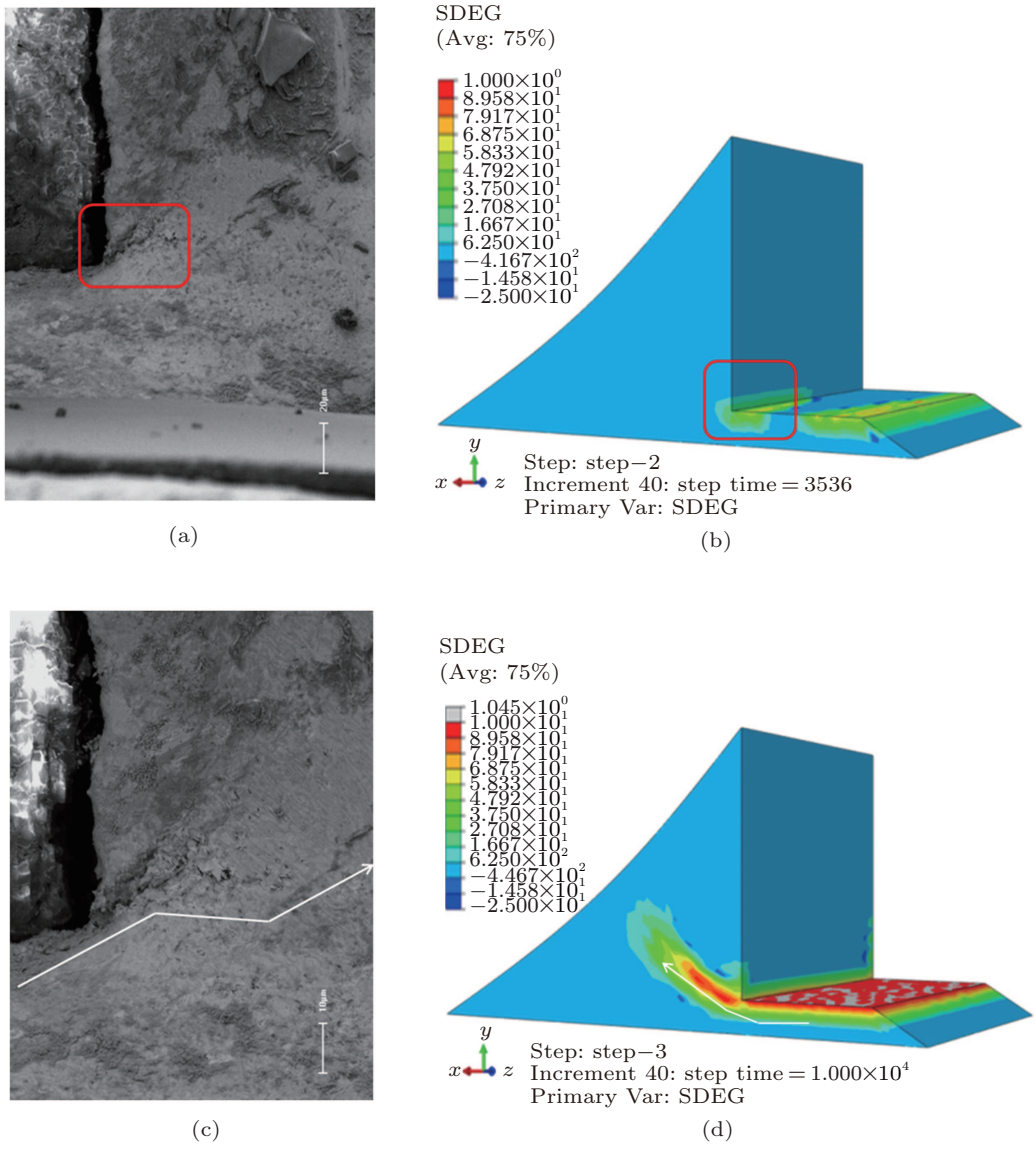



**Fig. 5.** (color online) SEM *in-situ* images and the FE simulation results after different cycles under the pull–pull axial cyclic loading. (a) and (c) $N = 6994$ and 10106, interface crack in the SEM *in-situ* testing; (b) and (d) $N = 3536$ and $1 \times 10^4$, interface damage in the FE simulation.

For the bending cyclic loading, the sample was placed horizontally, and the fatigue crack propagation behaviors were also observed. When the normal substrate stress is 70.0 MPa at $R = 0.1$ by using the SEM *in-situ* technology, the experimental results indicate that the fatigue crack initiation directly occurred at the heel location of the solder joint after several tens of thousand cycles, and the other crack along the substrate of PCB is initiated from the toe as shown in Fig. 6(a). Subsequently, the fatigue crack at the solder joint propagated about 155-μm length along the horizontal direction then it deflected at a larger angle with respect to the horizontal direction from about 45° to 55°–60° after from 98291 cycles to 205869 cycles, and the total fatigue crack length increased from 214 μm up to 367 μm as shown in Figs. 6(a) and 6(c). One reason for crack deflection is the effect of stress or strain concentrating in the region close to the heel of solder joint and the interaction of the crack with the interface between the chip and solder alloy. For the FE simulations, the evolution process of scalar stiffness degradation from the bottom to the solder free surface is clearly shown for push–push bending cyclic loading after $2 \times 10^4$ and $4 \times 10^5$ cycles, respectively. Besides the damage evolution near the toe and heel of the solder joint, another area of fatigue damage appearing at the bottom of the free oblique surface of the solder joint was ignored in the experimental investigation as shown in Fig. 6(b). Through numerical simulation, we can find that the two accumulating damages in the solder joint develop along the opposite directions, and they meet at the middle of the solder joint after $4 \times 10^5$ cyclic push–push bending loading; finally turning out to be complex and comprehensive as shown in Fig. 6(b). Although the crack initiation and propagation derived from the free oblique surface of the solder joint were not observed, the typical plastic zone on the surface of the solder joint in the experiment testified the rationality and accuracy of the FE fatigue analysis.

The displacement component $U_1$ at the center of the substrate bolt hole under axial tensile cyclic loading (see Fig. 3(a)) and the component $U_2$ at the upper punch die under 3-pont bending cyclic loading (see Fig. 3(b)) were output to describe the displacement alternation of the constraint node during $1 \times 10^5$ cycles as shown in Figs. 7(a) and 7(b). We can find that the damage extrapolation technique in the solder joint accelerates the fatigue damage process under the sine wave pulsating cyclic loading, and the mean displacement component $U_2$ is about 0.055 mm, and $U_1$ is about 0.016 mm.

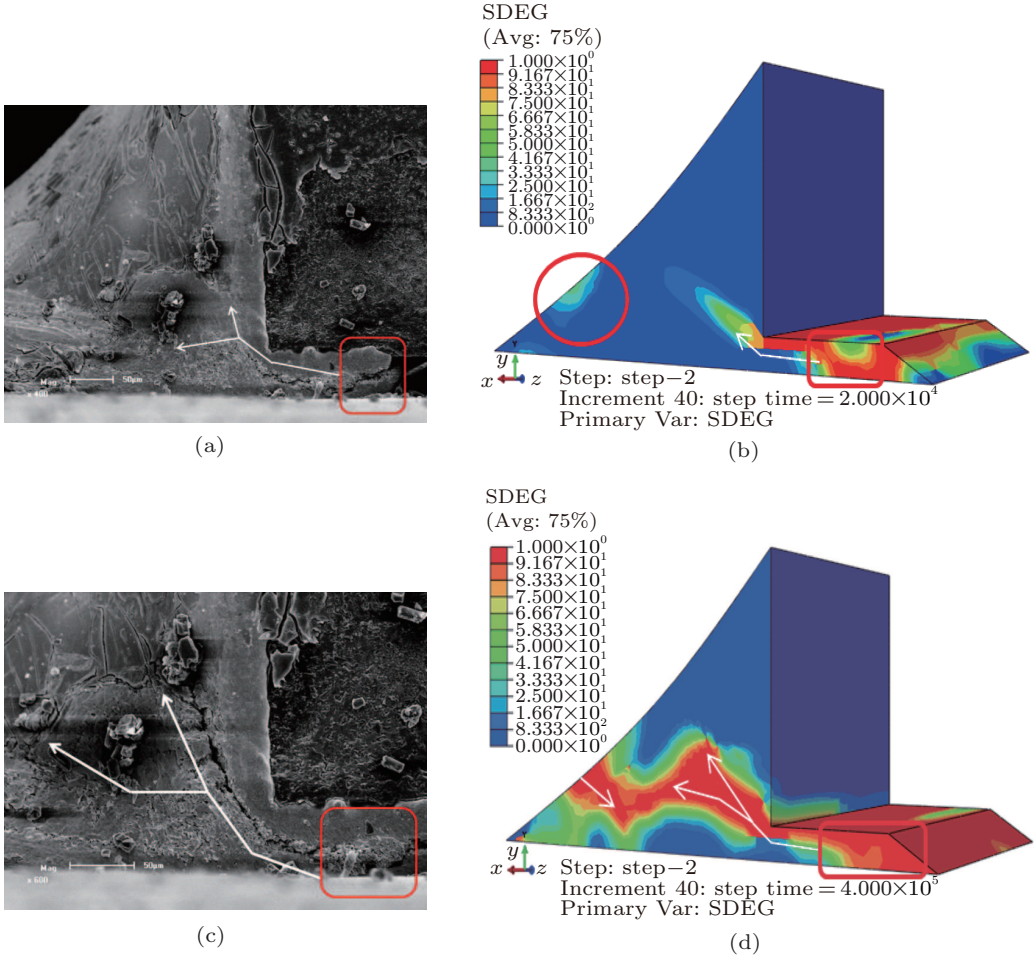



**Fig. 6.** (color online) SEM *in-situ* images and the FE simulation results after different cycles under the bending cyclic loading. (a) and (c) $N = 98291$ and 205869, interface crack in the SEM *in-situ* testing; (b) and (d) $N = 1 \times 10^4$ and $4 \times 10^5$, interface damage in the FE simulation.

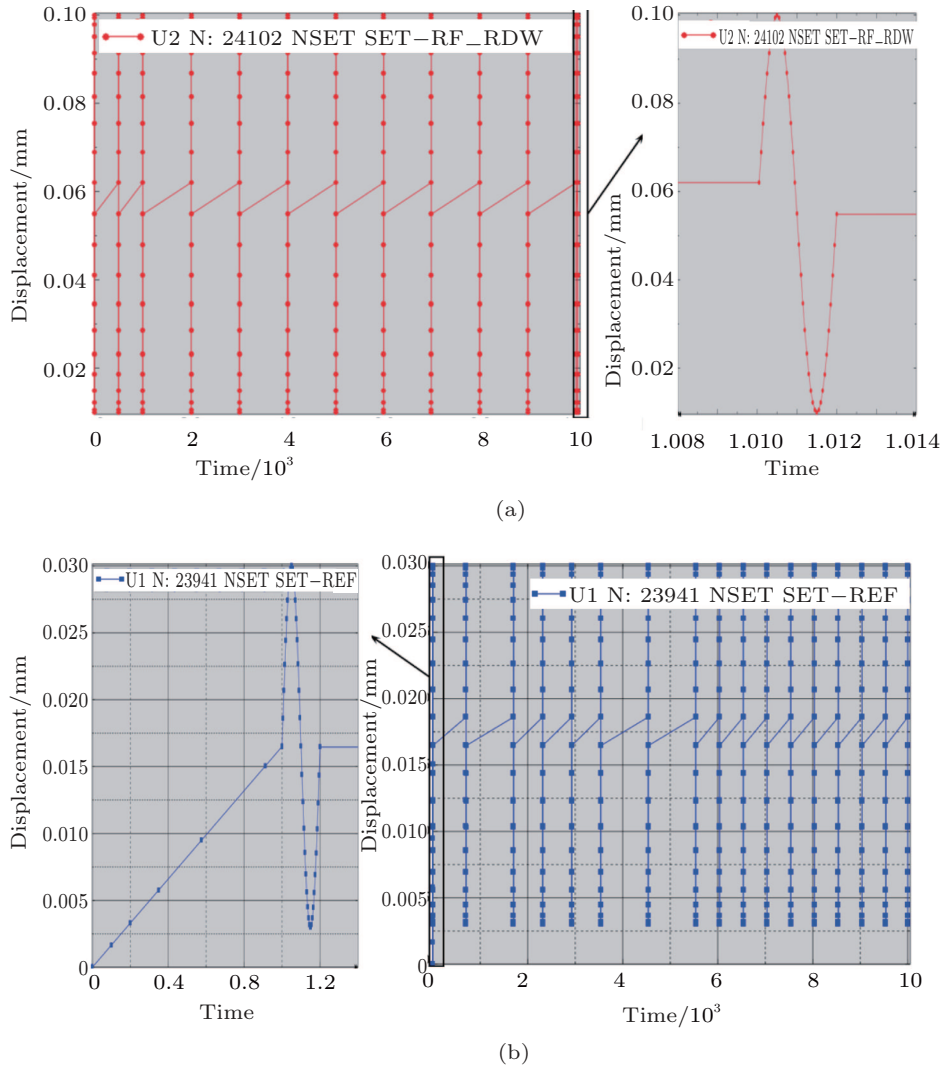



**Fig. 7.** (color online) Displacement alternation of the constraint node in two FE models during $1 \times 10^5$ cycles. (a) Displacement component $U_1$ at the center of substrate hole for the pull–pull loading, and (b) displacement component $U_2$ at the upper punch die for the bending cyclic loading.

By comparing the fatigue crack propagation behavior between push–push bending cyclic loading and pull–pull axial cyclic loading based on SEM *in-situ* technology, we can find that there are obvious differences in fatigue crack propagation path and crack growth rate in the solder joint at the same normal stress of substrate; in addition, the difference in fatigue crack initiation behavior between the two applied loadings is also obvious. As the results of fatigue cracking mechanisms, the path of fatigue crack propagation is always perpendicular to the maximum principal stress direction, which is affected by the shear stress component and the geometrical shape of the solder joint, especially the solder joint's skeleton map, so that the fatigue cracking driven force is very complex. The effects of different cyclic applied loads on the fatigue crack growth path in solder alloy cannot be ignored. It means that the fatigue crack propagation behavior in the maximum shear plane seems to be a governing mechanism at the tip of the crack. In addition, the accumulating damage based on FE fatigue life analysis under the different alternating stress loads can be used to predict the fatigue life and deduce the damage process of the solder joint very well.

## 5. Conclusions

The fatigue tests of a surface-mount electronic package for pull–pull axial cyclic loading and push–push bending cyclic loading in the HCF regime are conducted, and the fatigue crack initiation and propagation behaviors of the solder joint on a micro-scale are investigated based on SEM *in-situ* technology. Experimental results indicate that the position of fatigue crack initiation is different in detail and the fatigue cracks that reach several micrometers are described. A comparison of fatigue crack growth behavior between two different applied loads ($R = 0.1$) shows that there are obvious differences in fatigue crack propagation path and crack growth rate of a solder joint at the same stress level of the substrate based on the experimental observations. The propagation directions of these fatigue cracks deflect the direction of the applied load.

In addition, the simulation results for the fatigue damage process of solder joints with considering the constitutive model of damage initiation criteria and damage evolution

based on accumulating inelastic hysteresis energy are identical to the experimental results. Furthermore, the integrated and detailed fatigue damage evolution processes of the solder joint reveal that the position of fatigue crack initiation for the pull–pull cyclic loading occurs at the toe and heel of the interface between the chip and the solder joint, instead of at the heel of the solder joint for push–push cyclic loading. The variation range of maximum plastic strain is a main factor dominating the early stage of fatigue crack growth after $1.0 \times 10^5$ cycles at an applied stress level of 70.0 MPa on the substrate. There are very different threshold values of damage initiation and process of damage accumulation at the toe for two cyclic loadings, and the accumulation of equivalent plastic strain determines the trend and direction of fatigue crack propagation.

## References


[1] Kim D G 2006 *Microelectron. Eng.* **83** 2391
[2] Qu X 2007 *Microelectron. Reliab.* **47** 2197
[3] Wang X S 2008 *Int. J. Fracture* **151** 269
[4] Wang X S 2011 *Microelectron. Reliab.* **51** 1377
[5] Ročak D 2007 *Microelectron. Reliab.* **47** 986
[6] Erinc M 2007 *Int. J. Solids Struct.* **44** 5680
[7] Wang X S 2003 *Exp. Techniques* **27** 31
[8] Agrawal R and Espinosa H D 2009 *J. Micromech. Microeng.* **131** 41208
[9] Liu Z L, Hu H Y, Fan T Y and Xing X S 2009 *Chin. Phys. B* **18** 1283
[10] Lee W W 2000 *Microelectron. Reliab.* **40** 231
[11] Roellig M 2007 *Microelectron. Reliab.* **47** 187
[12] Wang X S and Fan J H 2004 *J. Mater. Sci.* **39** 2617
[13] Wang X S 2005 *Acta Metall. Sin.* **41** 1272
[14] Wang X S and Fan J H 2006 *Int. J. Fatigue* **28** 79
[15] Evans J W 2000 *Microelectron. Reliab.* **40** 1147
[16] Zhang L 2004 *Microelectron. Reliab.* **44** 5337
[17] Sun P 2006 *Solder. Surf. Mt. Tech.* **18** 4
[18] Lai Y S 2007 *Microelectron. Reliab.* **47** 111
[19] Huang J G 2007 *Mater. Trans.* **48** 2795
[20] Nayeb-Hashemi H and Yang P H 2001 *Int. J. Fatigue* **23** 325
[21] Xue Y 2007 *Eng. Fract. Mech.* **74** 2810
[22] Kanchanomai C 2005 *Mech. Mater.* **37** 1166